DSCC2020-3288

DYNAMIC PREDICTION-BASED OPTICAL LOCALIZATION OF A ROBOT DURING CONTINUOUS MOVEMENT

Jason N. Greenberg and Xiaobo Tan

Smart Microsystems Lab
Department of Electrical and Computer Engineering
Michigan State University
East Lansing, MI 48824
Email: green108@egr.msu.edu, xbtan@egr.msu.edu

ABSTRACT

Localization of mobile robots is essential for navigation and data collection. This work presents an optical localization scheme for mobile robots during the robot's continuous movement, despite that only one bearing angle can be captured at a time. In particular, this paper significantly improves upon our previous works where the robot has to pause its movement in order to acquire the two bearing angle measurements needed for position determination. The latter restriction forces the robot to work in a stop-and-go mode, which constrains the robot's mobility. The proposed scheme exploits the velocity prediction from Kalman filtering, to properly correlate two consecutive measurements of bearing angles with respect to the base nodes (beacons) to produce location measurement. The proposed solution is evaluated in simulation and its advantage is demonstrated through the comparison with the traditional approach where the two consecutive angle measurements are directly used to compute the location.

INTRODUCTION

Mobile robot localization in GPS denied environments such as underwater is a large field of research with many approaches to solving the challenge. Approaches vary based on factors such as the type of data used, how the data is captured and the algorithm that converts the measured data into position. For example, some of the varieties of observed data include distance, angle and

signal strength measurements, which can be captured by sensors such as sonar scanners, RF antenna, inertial sensors, and optical-based sensors, and then processed with techniques like SLAM (Simultaneous Localization and Mapping), dead-reckoning, triangulation, and trilateration [1–3].

Of the handful of the variations that can be used underwater, many are implemented with the use of acoustic signals, which is currently the predominant medium for underwater localization and communication. However, acoustic approaches tend to further complicate or constrain the localization algorithm due to the inherent limited bandwidth, long propagation delays, and multipath effect, which result in low data rates and low signal reception reliability [4, 5]. Moreover, devices that implement acoustic-based methods tend to be bulky and power-hungry, making them unsuitable for small underwater robots with limited resources [6].

Optical communication systems based on Light-Emitting Diodes (LEDs) are becoming a popular alternative to acoustic-based methods, due to their demonstrated ability to perform well in high-rate, low-power underwater communication over short-to-medium distances [7–10]. However, LED-based communication is limited by its requirement to have near line-of-sight (LOS) between the transmitter and the receiver. Fortunately, several solutions to this challenges have been presented, and include the use of redundant transmitters/receivers [11–14] and active alignment [8, 15, 16].

Indoor LED-based localization and communication systems

have been developed in the form of visible light communication (VLC) and visible light positioning (VLP) systems, where the the overhead lights used to illuminate the room can also be used as the transmission medium for both data and localization purposes [17, 18]. However, these approaches are not practical for a typical aquatic environment due to the difficulty in illuminating the significantly larger and more complex environment. An underwater LED-based localization and communication system was presented by Rust and Asada in [13]. This approach relies on a nonlinear light intensity model to calculate the distance between the transmitting LED and the receiving photodiode. However, such an approach is prone to error since light intensity depends on both distance and receiver-transmitter alignment. The method in [13] also uses a photodiode array to determine the angle of the light source, which increases the size and complexity of the system.

Our prior works [19-21] presented an approach to LEDbased Simultaneous Localization and Communication by taking advantage of the line of sight (LOS) requirement in LED-based communication to extract the relative bearing between a mobile robot and two nodes with known positions (referred to as base nodes). The bearing angles were then used to triangulate the position of the mobile robot. A Kalman filter was implemented to combat the challenge of measurement noises and to allow robot position prediction to facilitate the light scan for bearing measurement. However, this approach came with the assumption that the angles were captured when the mobile robot was at a single location. Consequently, because scanning for the light intensity with a rotating receiver cannot capture both angles simultaneously, our implementation used a stop-and-go motion in order to ensure the robot was at a single location. However, this significantly slowed the robots movement, making it unsuitable for time-sensitive tasks.

In this work, we propose a novel solution to LED-based localization which is capable of capturing the position of the robot while it is continuously moving. In particular, the proposed approach takes advantage of the estimated velocity from the Kalman filter, to properly correlate the two consecutive measurements of bearing angles with respect to the two base nodes for the position computation. In contrast to the previous works, this approach also now uses for the first time a rigid-body model to more accurately estimate the robot's movement. The performance of the proposed dynamic-prediction approach is evaluated in simulation in the measured body orientation and compared with the performance of the traditional approach used in our previous works, under the same noise conditions. The results show that the dynamic-prediction method does consistently better than the traditional method over a range of noise levels for the body orientation measurement.

The remainder of this paper starts with a basic concept of the LED-based localization scheme and outlines the Kalman filtering scheme used in robot state prediction. Then the proposed scheme is presented followed by a description of the simulation setup and results. Finally, concluding remarks and future work are provided.

OVERVIEW OF LED-BASED LOCALIZATION

To simplify the discussion, the localization approach is discussed in the two-dimensional (2D) space. All nodes have an optical transceiver, which is an LED transmitter together with a photodiode receiver. Each node is also able to rotate and monitor the orientation of its transceiver about the horizontal plane. This work assumes a network of 3 nodes, a pair of base nodes (with known locations), BN_1 and BN_2 , and a mobile node, MN, to be localized as illustrated in Figure 1.

The mobile node's coordinates can then be computed via the bearing angles θ_1 and θ_2 , and the known locations of the base nodes BN₁ and BN₂:

$$\begin{bmatrix} n_x \\ n_y \end{bmatrix} = \begin{bmatrix} B_{1x} + |V_1|\cos\theta_1 \\ B_{1y} + |V_1|\sin\theta_1 \end{bmatrix}$$
 (1)

where the x,y coordinate vectors for the MN and BN₁ are $\begin{bmatrix} n_x, n_y \end{bmatrix}^T$ and $\begin{bmatrix} B_{1x}, B_{1y} \end{bmatrix}^T$, respectively, and the magnitude of vector V_1 from Figure 1 is $|V_1|$, which is obtained via the Laws of Sines:

$$|V_1| = \frac{d\sin(\bar{\theta}_2)}{\sin(\theta_n)} \tag{2}$$

Here θ_n is the angle corresponding to the side BN₁-BN₂ within the MN-BN₁-BN₂ triangle, $\theta_n = \theta_2 - \theta_1$, $\bar{\theta}_2$ is the complement of θ_2 , $\bar{\theta}_2 = 180^{\circ} - \theta_2$, and d is the distance between BN₁ and BN₂.

Though the approach may appear straightforward, capturing accurate bearing angles is made non-trivial when the target node is mobile, since insufficient synchronization and coordination among the nodes can lead to improper LOS, thereby degrading both communication and angle measurements. Moreover, angle measurement error caused by inherent noise will lead to highly variable (as opposed to smooth) trajectory estimation for the MN, due to the reliance on pure algebraic calculation. Kalman filtering addresses these concerns by generating predicted positions of the MN to significantly reduce the scanning effort on all parties to facilitate LOS establishment, which then enhances localization accuracy and efficiency. A brief overview of the Kalman filter used in this work is discussed next.

Kalman Filtering Algorithm

In this work, the Kalman filter is used to help establish the LOS between the mobile node and base nodes, by predicting the

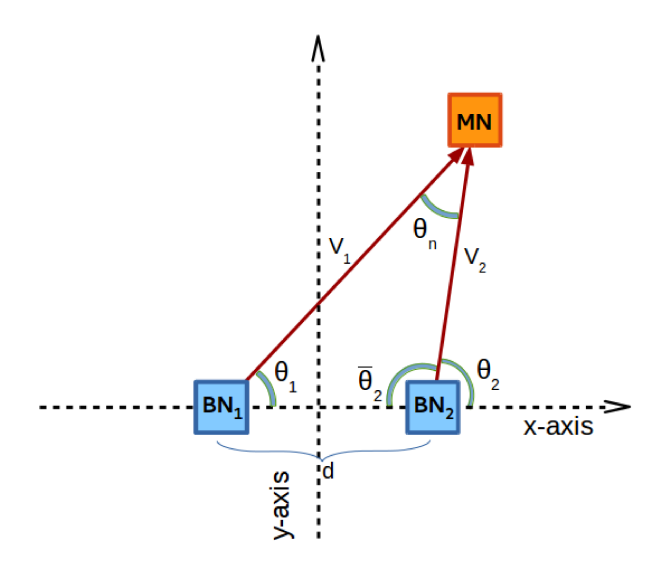


FIGURE 1. Illustration of the traditional localization approach [20].

future state of the robot so that the base nodes and mobile node can anticipate each other's angular locations. In our prior work, the mobile robot was modeled as a point mass, only focusing on the changes in x, y coordinates. In this work, we use a rigid-body model to represent the mobile node's motion, monitoring changes to both the body's orientation and the position. For both position and orientation, a constant (angular) velocity model corrupted with Gaussian noise is used for the mobile node's dynamics, since in general the precise knowledge of its movement is not known. These dynamics can be represented as:

$$\mathbf{n}_{k+1} = \mathbf{n}_k + \mathbf{v}_k \Delta_k + w_{1,k} \tag{3}$$

$$\mathbf{v}_{k+1} = \mathbf{v}_k + w_{2,k} \tag{4}$$

$$\psi_{k+1} = \psi_k + \omega_k \Delta_k + w_{3,k} \tag{5}$$

$$\omega_{k+1} = \omega_k + w_{4,k} \tag{6}$$

where $\mathbf{n}_k = \begin{bmatrix} n_{x,k}, n_{y,k} \end{bmatrix}^T$ and $\mathbf{v}_k = \begin{bmatrix} v_{x,k}, v_{y,k} \end{bmatrix}^T$ are the position and velocity vectors of the mobile node in terms of the x and y coordinates at the k-th time instance, ψ_k and ω_k are the body orientation angle and the body's angular velocity, respectively, $w_{1,k}$, $w_{2,k}$, $w_{3,k}$, and $w_{4,k}$ are independent, zero-mean, white Gaussian noises, and Δ_k is the k-th sampling interval. The observations \mathbf{z}_k and ζ_k are the noise-corrupted location and orientation measurements, respectively. They are represented as:

$$\mathbf{z}_k = \mathbf{n}_k + w_{5k},\tag{7}$$

$$\zeta_k = \psi_k + w_{6,k},\tag{8}$$

where $w_{5,k}$ and $w_{6,k}$ are assumed to be white, zero-mean Gaussian, and independent of each other and the process noises $w_{1,k}$,

 $w_{2,k}$, $w_{3,k}$, and $w_{4,k}$.

 \mathbf{z}_k is computed from (1) and (2), which is only possible in physical implementation when the bearing angles, θ_1 and θ_2 , are measured by the MN at a single fixed position. The main focus of this work addresses how \mathbf{z}_k can be computed when the bearing angles are captured by the mobile node at different positions due to the robot's movement.

 ζ_k is measured from an orientation sensor such as a magnetic compass. Body orientation estimation is needed for the mobile robot to compute the required rotation for the transceiver to establish the LOS, by properly accommodating the rotation of the robot itself.

Two state vectors are used for Kalman filtering in this work. The first state vector, $\hat{\mathbf{x}}_k$, maintains the estimate of the position and velocity, whereas the second state vector, $\hat{\mathbf{b}}_k$, tracks the estimate of the body orientation angle and the angular velocity. The two state vectors are defined as

$$\hat{\mathbf{x}}_k = \left[\hat{n}_x, \, \hat{n}_y, \, \hat{v}_x, \, \hat{v}_y\right]^T \tag{9}$$

$$\hat{\mathbf{b}}_k = [\hat{\boldsymbol{\psi}}, \, \hat{\boldsymbol{\omega}}]^T \tag{10}$$

where $[\hat{n}_x, \hat{n}_y]^T$, $[\hat{v}_x, \hat{v}_y]$, $\hat{\psi}$, and $\hat{\omega}$ are the estimated position, velocity, body orientation angle, and angular velocity of the mobile node at the k-th time instance, respectively. The equations for the implementation of the Kalman filter, which are standard [22], are omitted here for brevity.

At time k, the predicted position from the state estimate $\hat{\mathbf{x}}_{k+1}^-$ is used to determine anticipated values for the bearings θ_1 and θ_2 (recall Figure 1) that will be used in the angular scanning process that ultimately results in the position observation \mathbf{z}_k used in the state estimate update. Anticipated angles $\hat{\theta}_{1,k+1}$ and $\hat{\theta}_{2,k+1}$ of the mobile node relative to the base nodes are computed by using

$$\hat{\theta}_{i,k+1} = \cos^{-1}\left(\frac{V_{b_i} \cdot V_{m_i}}{|V_{b_i}| |V_{m_i}|}\right), \text{ for } i = 1,2$$
 (11)

where,

$$V_{b_1} = \begin{bmatrix} 0 \\ 0 \end{bmatrix} - \begin{bmatrix} B_{1x} \\ B_{1y} \end{bmatrix} \tag{12}$$

$$V_{b_2} = \begin{bmatrix} B_{2x} \\ B_{2y} \end{bmatrix} \tag{13}$$

$$V_{m_i} = \begin{bmatrix} \hat{n}_x^- \\ \hat{n}_y^- \end{bmatrix} - \begin{bmatrix} B_{ix} \\ B_{iy} \end{bmatrix}, \text{ for } i = 1, 2$$
 (14)

In these equations $[B_{1x}, B_{1y}]$ and $[B_{2x}, B_{2y}]$ are the respective x and y coordinates for base nodes BN₁ and BN₂ and $V_{b_i} \cdot V_{m_i}$ is

the dot product between vectors V_{m_i} and V_{b_i} . The mobile node and base nodes each have their own sets of anticipated angles for use in the measurement process, with the mobile node using its angles as a basis for where to start and end its scanning rotation, and the base nodes centering their LED light about their set of angles.

Challenges With Continuously Moving Robot

The traditional measurement system, (1) and (2), used in our previous works assumed that the bearing angles were captured when the mobile robot was at a single fixed position. Consequently, because the physical angle scanning process takes time, i.e., it is not physically possible to instantaneously capture both angles with a rotating transceiver, it required the mobile node's trajectory to be executed in a stop-and-go manner in order to ensure that the robot was at the same position for both angle captures.

As beneficial as it is, the stop-and-go implementation is time-consuming and thus limits how quickly the robot can traverse its environment, making it unsuitable for time-sensitive tasks. In this work we propose an approach that allows the robot to localize while also moving continuously in its environment. That is, we propose an algorithm that can compute the robot's position despite the fact that the two consecutive measurements of bearing angles, with respect to the two base nodes, are captured at different times and positions.

PROPOSED APPROACH

The bearing angles, θ_1 and θ_2 , are captured by the MN while it moves along its trajectory, where each angle is captured at a distinct position along this path. These spotting positions are labeled as P_a and P_b , where P_a is the position whose *x*-coordinate is the smallest and not necessarily the position where the first bearing angle is spotted. Localization of the robot is achieved by determining the coordinates of these spotting positions, and treating one these positions as the observed location \mathbf{z}_k of the robot.

The concept for calculating these positions is considerably more involved than the traditional approach described in (1) and (2). To better contrast their differences, Figure 2 illustrates how the two approaches would determine a position given the same measured bearing angles. In particular, the diagram shows that the traditional approach would use the two angles to find a converging point at P_f , which is significantly distant from the two ground-truth locations, P_a and P_b , where the angles were actually captured by the robot. Moreover, with access to only the bearing angles, the coordinates for P_a and P_b could be any of the points along the two edges of the triangle formed by P_f , BN_1 , and BN_2 . To determine an estimate of the positions for P_a or P_b , this work exploits the MN's most recently estimated velocity to

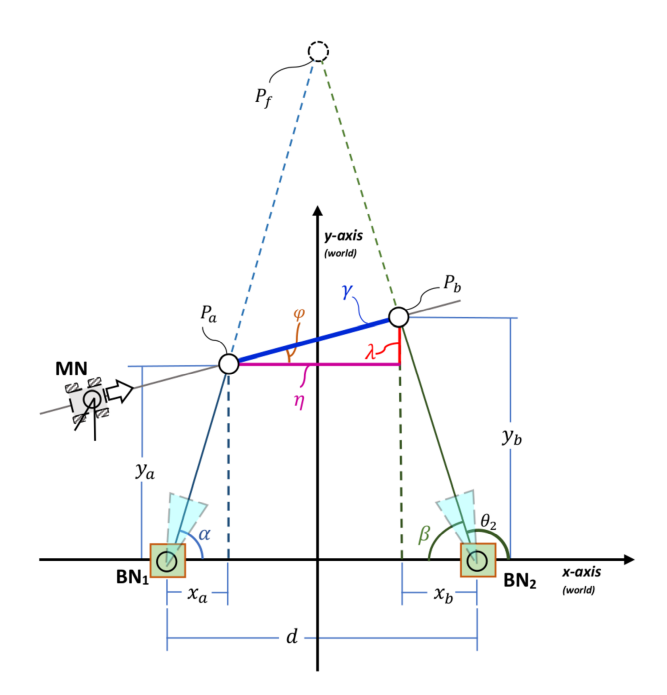


FIGURE 2. Illustration comparing the traditional approach and the proposed dynamic-prediction approach, for the case when θ_1 and θ_2 are at spots P_a and P_b , respectively.

properly combine the two measured angles.

Measurement Equations

The locations of the mobile node, P_a and P_b , where it spotted a bearing angle can be determined by solving for the x and y distances between each spot location and the base node of the corresponding captured angle, by using these angles along with the estimated velocity of the mobile node. For instance, in Figure 2, BN_1 and P_a are separated from each other by x_a and y_a . Similarly, BN_2 and P_b are related by x_b and y_b . These distances can be expressed in generalized mathematical relationships as:

$$P_{ax} = BN_{1x} + \mathbf{A}x_a \tag{15}$$

$$P_{bx} = BN_{2x} + \mathbf{B}x_b \tag{16}$$

$$P_{ay} = BN_{1y} + \mathbf{C}y_a \tag{17}$$

$$P_{by} = BN_{2y} + \mathbf{D}y_b \tag{18}$$

where P_{ax} , P_{bx} and P_{ay} , P_{by} are the x and y coordinates of P_a and P_b , respectively, BN_{1x} , BN_{2x} and BN_{1y} , BN_{2y} are the x and y coordinates of BN_1 and BN_2 , respectively, and A, B, C, and D are the sign values of the distances x_a , x_b , y_a and y_b , respectively. A, B, C, and D reflect where the spot locations are relative to the base nodes, and can be determined by inspecting the properties of the captured bearing angles. In particular, A and B take on the

sign value of $\cos \theta_1$ and $\cos \theta_2$, respectively, and **C** and **D** take on the sign value of $\sin \theta_1$ and $\sin \theta_2$, respectively.

From the relationships in (15) - (18), expressions for the distances x_a , x_b , y_a and y_b can be derived as:

$$x_{a} = \frac{d - \eta + \mathbf{BE} \frac{\gamma \sin \varphi}{\tan \beta}}{\mathbf{A} - \mathbf{B} \frac{\tan \alpha}{\tan \beta}}$$
(19)

$$y_a = x_a \tan \alpha \tag{20}$$

$$y_b = y_a + \mathbf{E}\lambda \tag{21}$$

$$x_b = \frac{y_b}{\tan \beta} \tag{22}$$

where,

$$d = BN_{2x} - BN_{1x} \tag{23}$$

$$\eta = \gamma \cos \varphi \tag{24}$$

$$\lambda = \gamma \sin \varphi \tag{25}$$

$$\rho = \begin{cases} +1, & (0^{\circ} \le \varphi < 90^{\circ}) \\ -1, & (-90^{\circ} < \varphi < 0^{\circ}) \end{cases}$$
 (26)

$$\mathbf{E} = \begin{cases} (\boldsymbol{\rho} = +1) \wedge (\mathbf{C} = +1) \wedge (\mathbf{D} = +1) \\ +1, & \vee \\ (\boldsymbol{\rho} = -1) \wedge (\mathbf{C} = -1) \wedge (\mathbf{D} = -1) \end{cases}$$

$$(27)$$

$$(\boldsymbol{\rho} = -1) \wedge (\mathbf{C} = +1) \wedge (\mathbf{D} = +1)$$

$$-1, & \vee \\ (\boldsymbol{\rho} = +1) \wedge (\mathbf{C} = -1) \wedge (\mathbf{D} = -1)$$

In these equations, d is the distance between the base nodes, η is the x-distance between the spotted points, i.e., the distance from P_a to P_b , and λ is the y-distance between the spotted points with E being its associated sign value, which is determined from a combination of the slope, ρ , and the sine values of the bearing angles. The variables α and β represent the inner angles of the triangles that each base node makes with its corresponding spotting point and are computed from θ_1 and θ_2 , respectively, and γ and φ are the magnitude and angle of the Kalman filter-estimated velocity of the mobile node's movement, respectively. To simplify the discussion, it is assumed, without loss of generality, that the base nodes are separated only along the x-axis. By using the two sets of relationships (15) - (18) and (19) - (22) the position of P_a (or P_b) can be computed and then used in the Kalman filter's state estimate update.

The above relationships, (15) – (22), were developed from the situation shown in Figure 2, where θ_1 and θ_2 are captured at spots P_a and P_b , respectively. In the case where θ_1 and θ_2

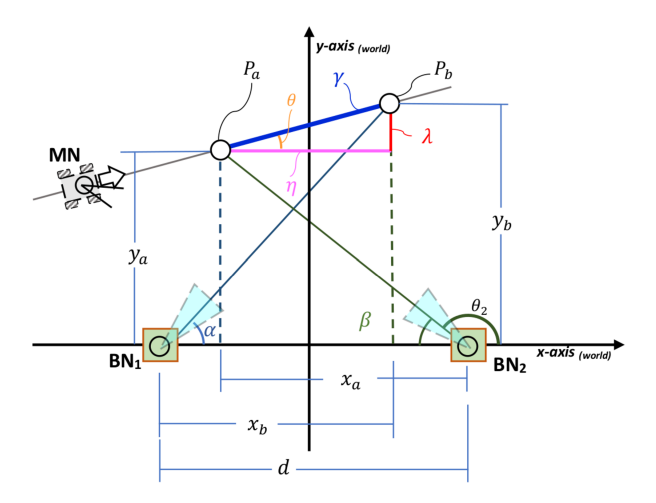


FIGURE 3. Illustration of the moving measurement approach, which shows the situation when θ_1 and θ_2 are at spots P_b and P_a , respectively.

are alternatively captured at spots P_b and P_a , respectively, as is illustrated in Figure 3, equations (15) – (22) would be simply adjusted to reflect the new association between the angles spot positions and the base nodes.

SIMULATION SETUP

The proposed dynamic-prediction algorithm was evaluated in simulation and its performance was compared to the traditional approach to computing the measured position. In particular, the robustness of both approaches was tested against measurement error in the body orientation, which results in error in bearing angle measurement.

The robot's performance was evaluated with a closed loop trajectory as shown in Figure 4. The trajectory was defined in terms of a number of position points, which were used as the ground-truth positions in the simulation. Base nodes BN_1 and BN_2 were positioned at $[-1,0]^T$ and $[1,0]^T$, respectively.

Simulated Measurements

The simulated robot body orientation measurement was generated by adding zero-mean Gaussian noise to the ground truth orientation value. The simulated ground truth body orientation of the mobile node was obtained by finding the angle between the 0° orientation vector and the vector that points from the previous to the current ground truth position. The amount of error in the orientation measurement was controlled by adjusting the standard deviation of the Gaussian noise.

The Kalman filter-estimated body orientation (based on the body orientation measurement) was used to adjust the mobile node's transceiver angle in order to establish LOS by properly

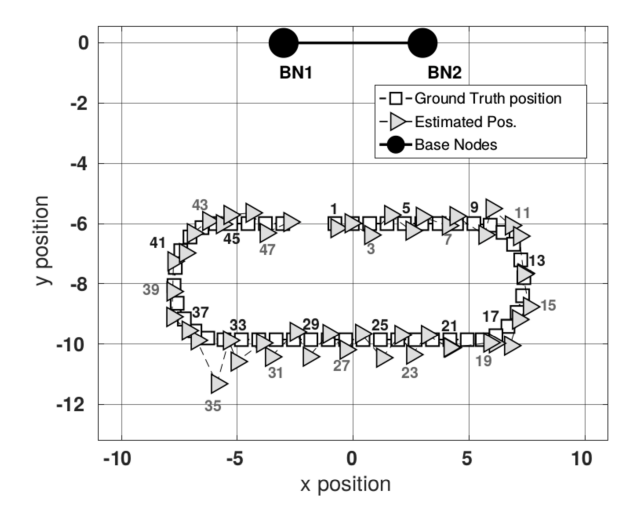


FIGURE 4. Comparison of the ground truth and estimated positions for one of the simulated trials using the loop trajectory, for the case when the body orientation angle measurement is subjected to Gaussian noise with a standard deviation of 1.00° .

accommodating the robot's own rotation. The error in the estimated orientation angle had the effect of eschewing the scanned light intensities thus resulting in errors in the angle error.

Angle measurements were generated by simulating the process of the MN scanning the light intensities shown by the base nodes. The range of the mobile node's scan was the angular distance between the predicted angles, $\hat{\theta}_{1,k+1}$ and $\hat{\theta}_{2,k+1}$, computed in (11), plus an additional 30° in the opposite direction of each angle. The scan resolution was set to a step size of 0.225° , to mimic the rotation resolution of the stepper motor used in the hardware implementation of our previous works. The amount of time that elapsed between the steps of the scan was determined by dividing the ground truth amount of time that elapses between the start and end of scan by the number of steps in the current range of rotation. The ground truth amount of time that elapses between the start and end of the scan was determined by taking the average time lapse between the start and end of scans from a small set of preliminary hardware tests.

The strength of the artificial light intensities were based on the degree of LOS achieved between the transceivers of the mobile node and the base nodes at each step of the mobile node's transceiver rotation. This degree of LOS, which ranged from [0.0, 1.0] with a value of 1.0 representing direct LOS, was first scaled by 7.3 to mimic the range of voltages measured by the photodiode, and was then injected with zero-mean Gaussian noise with a standard deviation of 0.5 volts to represent the inherent error associated with the light measuring process. The bearing angles were extracted from the simulated light intensities by determining the angular position of mobile node's transceiver at the center point of the two peaks in the intensity scan.

SIMULATION RESULTS

For all of the simulation results presented here the standard deviation of the body orientation error was varied from 1.0° to 5.0° in increments of 1.0° . For each level of standard deviation, 100 trials were conducted, where 100 random seeds were chosen to ensure the randomness would be repeatable for each of the cases. Figure 4 compares the ground truth and estimated positions in the x,y plane in one sample run for the loop trajectory, when the amount of standard deviation of Gaussian noise applied to the body orientation measurement was 1.00° .

Figures 5 and 6 show the average estimated error and the number of completed trials, respectively, for (a) the proposed dynamic-prediction approach when the ground truth velocity between the spotting points is used for the measurement equation, (b) the proposed dynamic-prediction approach when the predicted-velocity between the spotting points is used for the measurement equation, and (c) for the traditional approach where the two bearing angles were treated as being obtained from the same location. For the data shown in Figure 6, a trial was considered completed if the system was able to localize the mobile node's position at each and every trajectory step. The results in these figures show that in general the proposed dynamic-prediction approach performs better than the traditional approach; however, there is still clearly room for us to improve as the dynamic-prediction approach with the ground truth velocity does the best out of all 3 variations. In particular, while the performance of the dynamic-prediction approach using the predict-velocity does better than the traditional approach, it is not as nearly good as the version which uses the ground truth velocity. It is believed that the discrepancy in performance is caused by poor velocity estimates, to be improved upon for future work.

CONCLUSION

In this paper we have proposed an approach to LED-based localization of a continuously moving robot. By utilizing the estimated velocity of the mobile robot we were able to address the main challenge of measuring the robot's position despite the bearing angles being measured at different times and positions.

It was shown in simulation that the proposed dynamic-prediction approach was capable of localizing the mobile robot despite the bearing angles being captured at different times and locations. In addition, it also performed better than the traditional approach, which assumed the bearing angles were measured at a single location, for a single closed loop trajectory and under various levels of body orientation measurement noise.

Despite the successful results from the current simulation, there is still clear evidence that the approach can be refined further to yield more accurate results. Moreover, this system is limited to configurations where the MN is not collinear with the base nodes, as otherwise a singularity issue arises, resulting in ambiguity of the measured position. In [23] we proposed a localiza-

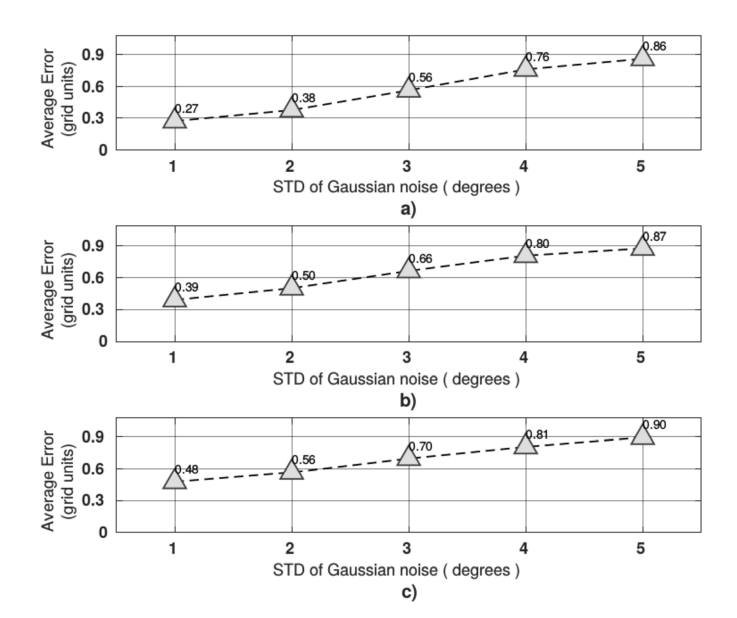


FIGURE 5. Average estimated position errors computed among all of the trials for varying amounts of standard deviation in the Gaussian noise added to the body orientation measurements of the mobile node. Estimated position error is the difference between the ground truth and the position from the Kalman filter's state vector $\hat{\mathbf{x}}_k = [\hat{n}_x, \hat{n}_y]$ after processing the observed position \mathbf{z}_k . Subplot a) shows the average error for the proposed dynamic-predication approach when the ground truth velocity between the two spotting points was used in the measurement equation. Subplot b) shows the average error for the proposed dynamic-predication approach when the predicted-velocity between the two spotting points was used in the measurement equation. Subplot c) shows the average error for the traditional approach.

tion approach which was capable of tracking the mobile robot when it is at or near a collinear configuration by using more base nodes which are strategically placed to provide alternative measurements perspectives in these cases. In future work this multiple base node approach will be extended to adopt the dynamic-prediction measurement system as proposed in this work. Additional future work will explore testing this approach in more complicated trajectories, such as the figure-8 shape, as well as implementing the scheme in hardware. Eventual goals for this work also include expanding to a 3D setting and using water-proofed hardware for underwater experimentation.

ACKNOWLEDGMENT

This work was supported in part by the National Science Foundation (IIS 1734272).

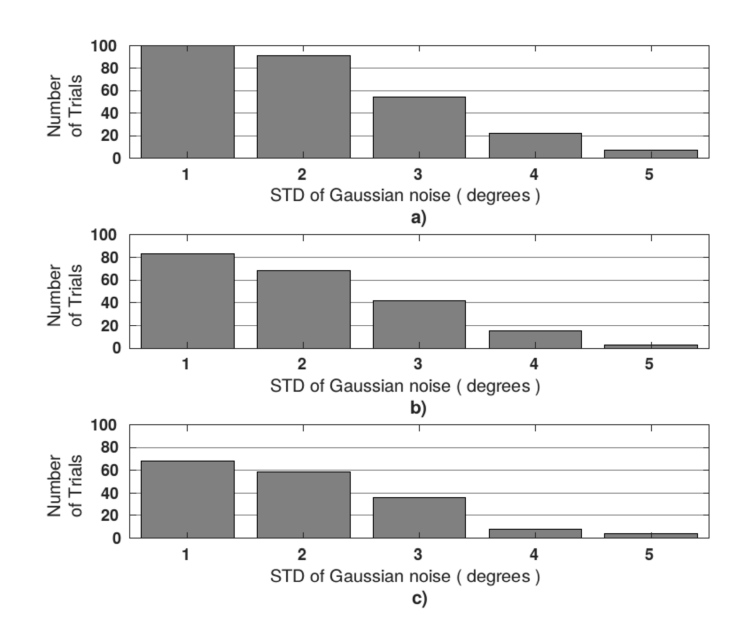


FIGURE 6. Bar graph showing how many of the 100 simulated trials for the loop trajectory were able to track the mobile node for the complete trajectory for each level of standard deviation of the Gaussian noise added to the body orientation measurements of the mobile node. Subplot a) shows the results for the proposed dynamic-predication approach when the ground truth velocity between the two spotting points was used in the measurement equation. Subplot b) shows the results for the proposed dynamic-predication approach when the predicted-velocity between the two spotting points was used in the measurement equation. Subplot c) shows the results for the traditional approach.

REFERENCES

- [1] Bergen, M. H., Jin, X., Guerrero, D., Chaves, H. A. L. F., Fredeen, N. V., and Holzman, J. F., 2017. "Design and implementation of an optical receiver for angle-of-arrival-based positioning". *Journal of Lightwave Technology*, **35**(18), Sept., pp. 3877–3885.
- [2] Bergen, M. H., Schaal, F. S., Klukas, R., Cheng, J., and Holzman, J. F., 2018. "Toward the implementation of a universal angle-based optical indoor positioning system". *Frontiers of Optoelectronics*, *11*(2), Jun., pp. 116–127.
- [3] A. F. Browne, and S. T. Padgett, 2018. "Novel method of determining vehicle cartesian location using dual active optical beacons and a rotating photosensor". *IEEE Sensors Letters*, 2(4), Dec., pp. 1–4.
- [4] Rui, G., and Chitre, M., 2016. "Cooperative multi-AUV localization using distributed extended information filter". In 2016 IEEE/OES Autonomous Underwater Vehicles (AUV), pp. 206–212.
- [5] Emokpae, L. E., DiBenedetto, S., Potteiger, B., and Younis, M., 2014. "UREAL: Underwater reflection-

- enabled acoustic-based localization". *IEEE Sensors Journal*, **14**(11), November, pp. 3915–3925.
- [6] Tan, X., 2011. "Autonomous robotic fish as mobile sensor platforms: Challenges and potential solutions". *Marine Technology Society Journal*, **45**(4), July, pp. 31–40.
- [7] Tian, B., Zhang, F., and Tan, X., 2013. "Design and development of an LED-based optical communication system for autonomous underwater robots". In Advanced Intelligent Mechatronics (AIM), 2013 IEEE/ASME International Conference on, pp. 1558–1563.
- [8] Solanki, P. B., Al-Rubaiai, M., and Tan, X., 2016. "Extended Kalman filter-aided alignment control for maintaining line of sight in optical communication". In 2016 American Control Conference, pp. 4520–4525.
- [9] Brundage., H., 2010. "Designing a wireless underwater optical communication system". Master's thesis, Massachusetts Institute of Technology.
- [10] Doniec, M., 2013. "Autonomous underwater data muling using wireless optical communication and agile AUV control". PhD thesis, Massachusetts Institute of Technology.
- [11] Anguita, D., Brizzolara, D., and Parodi, G., 2009. "Building an underwater wireless sensor network based on optical: Communication: Research challenges and current results". In 2009 Third International Conference on Sensor Technologies and Applications, pp. 476–479.
- [12] Anguita, D., Brizzolara, D., and Parodi, G., 2010. "Optical wireless communication for underwater wireless sensor networks: Hardware modules and circuits design and implementation". In OCEANS 2010, pp. 1–8.
- [13] Rust, I. C., and Asada, H. H., 2012. "A dual-use visible light approach to integrated communication and localization of underwater robots with application to non-destructive nuclear reactor inspection". In Robotics and Automation (ICRA), 2012 IEEE International Conference on, pp. 2445–2450.
- [14] Simpson, J. A., Hughes, B. L., and Muth, J. F., 2012. "Smart transmitters and receivers for underwater free-space optical communication". *IEEE Journal on Selected Areas in Communications*, *30*(5), June, pp. 964–974.
- [15] Al-Rubaiai, M., 2015. "Design and development of an LED-based optical communication system". Master's thesis, Michigan State University.
- [16] Solanki, P. B., Al-Rubaiai, M., and Tan, X., 2018. "Extended Kalman filter-based active alignment control for LED optical communication". *IEEE/ASME Transactions on Mechatronics*, 23(4), August, pp. 1501–1511.
- [17] Qiu, K., Zhang, F., and Liu, M., 2016. "Let the light guide us: VLC-based localization". *IEEE Robotics & Automation Magazine*, 23(4), December, pp. 174–183.
- [18] Nguyen, N. T., Nguyen, N. H., Nguyen, V. H., Sripimanwat, K., and Suebsomran, A., 2014. "Improvement of the VLC localization method using the extended Kalman fil-

- ter". In TENCON 2014 2014 IEEE Region 10 Conference, pp. 1–6.
- [19] Greenberg, J. N., and Tan, X., 2016. "Efficient optical localization for mobile robots via Kalman filtering-based location prediction". In Proceedings of the ASME 2016 Dynamic Systems and Control Conference. DSCC2016-9917.
- [20] Greenberg, J. N., and Tan, X., 2017. "Kalman filtering-aided optical localization of mobile robots: System design and experimental validation". In Proceedings of the ASME 2017 Dynamic Systems and Control Conference. DSCC2017-5368.
- [21] Greenberg, J. N., and Tan, X., 2020. "Dynamic optical localization of a mobile robot using kalman filtering-based position prediction". *IEEE/ASME Transactions on Mechatronics*. To Appear.
- [22] Kalman, R. E., 1960. "A new approach to linear filtering and prediction problems". *Transactions of the ASME–Journal of Basic Engineering*, 82(Series D), pp. 35–45.
- [23] Greenberg, J. N., and Tan, X., 2019. "Optical localization of a mobile robot using sensitivity-based data fusion". In 2019 IEEE/ASME International Conference on Advanced Intelligent Mechatronics (AIM), pp. 778–783.